

# An efficient method to calculate the complex $\vec{k}$ -space from simulation data

Alexander Blinne,<sup>1,\*</sup> Stephan Kuschel,<sup>1,2</sup> Stefan Tietze,<sup>1</sup> and Matt Zepf<sup>1,2,3</sup>

<sup>1</sup>*Helmholtz-Institut Jena, Fröbelstieg 3, D-07743 Jena, Germany*

<sup>2</sup>*Institute for Optics- and Quantumelectronics, Friedrich Schiller University Jena, Max-Wien-Platz 1, 07743 Jena, Germany*

<sup>3</sup>*Department of Physics and Astronomy, Queen's University Belfast, Belfast, BT7 1NN, UK*

A novel method for the analysis of real-valued electromagnetic field data from simulations is presented in this paper. As each component is a distinct dataset, their propagating interplay is often ignored. Reconstructing the complex  $k$ -space is often deemed too complicated and not expected to give much insight. With the new method presented here this changes, as it is a simple and efficient method to gain access to the full physical information of the electromagnetic fields from a single data dump. This allows counterpropagating plane waves to be accurately distinguished and to compute their complex coefficients independently. From these amplitudes, the complex-valued electromagnetic fields can be calculated from which information about phase and amplitude is readily available. Additionally, the complex fields allow for efficient vacuum propagation allowing to calculate far field data or boundary input data from near field data. An implementation of the new method is available as part of PostPic<sup>a</sup>, a data analysis toolkit written in the Python programming language.

## I. INTRODUCTION

Whenever the physics of some phenomenon or technique becomes so complex, that it cannot be handled using pen and paper or even numerical solutions of analytic equations, physicists will turn towards simulations. This is true across most sections of physics, including, but not limited to, astrophysics, hydrodynamics, laser physics, plasma physics, material sciences or even quantum physics. Many of these simulations include charged particles, surfaces or bulk materials, that interact with electromagnetic fields. Since most simulations try to model real-world physical setups, they give access to the electromagnetic fields  $E_{x,y,z}$  and  $B_{x,y,z}$  as real variables on a grid. This especially includes Particle in Cell (PIC) simulations [3, 4] which are being heavily used in laser and plasma physics. While looking at any of these fields directly may already give a lot of insight on what is happening during the simulation, much more information can be extracted when the full physical meaning of the electromagnetic field as a whole is taken into account. The simplest example for the additional information that can be gained access to is the differentiation between incident and outgoing waves, even when they are superposed and counterpropagating. Other examples include direct access to the complex field data, i.e. envelope and phase data.

The available techniques that give access to the full complex  $\vec{k}$ -space have some drawbacks which explains why they are not yet in widespread use. One approach would be to look at the fields in two consecutive dumps, which gives access to the temporal derivative of the fields. The problem with this approach is that most simulation codes are not typically set-up to dump their data in

that way, which may lead to the necessity to change the simulation code. Another approach is based on storing the fields on one plane, but at equal temporal intervals throughout the simulation. Similar problems apply here, such as the code not being able to dump information in that manner, which would lead to dumping far too much data far too often, slowing down the simulation and wasting disk space.

Let us use, as an example, a simulation of surface high harmonic generation (SHHG) [5–10]. This is a process, where a laser pulse is reflected off a plasma surface which, due to the light pressure of the incident laser, is moving at relativistic speeds. Due to the Doppler shift induced by this rapid motion, the reflected pulse will contain high harmonics.

Usually three things are important in these kinds of simulations:

1. the incident laser pulse,
2. the outgoing waveform and
3. the motion of the plasma particles during the interaction.

The incident and outgoing electromagnetic fields are, during the interaction, spatially superposed and the superposed field data at these times is usually discarded.

In the one-dimensional case it is obvious, that the waves propagating in either direction can be separated using information from only a single dump by the linear combinations

$$E_y^+ = \frac{1}{2} (E_y + cB_z) \quad E_y^- = \frac{1}{2} (E_y - cB_z), \quad (1)$$

which is true in both, spatial domain and frequency domain. We show, that it is possible to extend this method into the three dimensional frequency domain and separate the incident and outgoing waves in the data using just a single dump. By separating the waves propagating

\* [alexander.blinne@uni-jena.de](mailto:alexander.blinne@uni-jena.de)

<sup>a</sup> See [1, 2]

in the  $\vec{k}$  and  $-\vec{k}$  direction, we effectively reconstruct the complex  $\vec{k}$ -space of any or all component(s) of the electromagnetic field. This is different from a simple Fourier transform of the real data where the amplitudes for  $\vec{k}$  and  $-\vec{k}$  would be Hermitian conjugates making both propagation directions indistinguishable, which is not the case in the reconstructed, complex  $\vec{k}$ -space. Here, the amplitudes for  $\vec{k}$  and  $-\vec{k}$  are completely independent and refer directly to plane waves propagating in either direction with known amplitude and phase. An inverse Fourier transform of the complex  $\vec{k}$ -space will yield a complex field in spatial domain whose real part is, up to round-off errors, identical to the real field that the process was started with. From these complex, spatial data it is easy to access the envelope and spatial phase of the waveform.

By applying an additional phase  $\Delta\varphi = e^{-i\omega(\vec{k})t}$  to the complex  $\vec{k}$ -space data, it is trivial to perform additional vacuum propagation of the field. This is useful to gain access to far field information which spans a bridge to experimental data from, e.g., wavefront sensors.

If this method is applied not to a simulation dump, but to a model of the fields of a laser focus, it is possible to calculate the boundary input data for a simulation that recreates that exact focus on target. This is especially useful if analytic solutions for the propagation of fields of the desired focus are not available.

## II. ELECTROMAGNETIC PLANE WAVES

The electromagnetic fields  $\vec{E}(\vec{r}, t)$  and  $\vec{B}(\vec{r}, t)$  can be defined in terms of the vector potential  $\vec{A}(\vec{r}, t)$  and a scalar potential  $\varphi(\vec{r}, t)$ . The fields can be calculated from these potentials using the well known relations

$$\vec{E} = -\vec{\nabla}\varphi - \frac{\partial\vec{A}}{\partial t} \quad \vec{B} = \vec{\nabla} \times \vec{A}, \quad (2)$$

which guarantee

$$\vec{\nabla} \cdot \vec{E} = 0 \quad \vec{\nabla} \cdot \vec{B} = 0. \quad (3)$$

Because this method is targeted on fields in a vacuum, we can write a complete ansatz for the vector potential in radiation gauge  $\vec{\nabla} \cdot \vec{A} = \varphi = 0$  as

$$\vec{A}(\vec{r}, t) = \int d^3k \vec{A}_k(\vec{r}, t) \quad (4)$$

$$\vec{A}_k(\vec{r}, t) = \sum_{i=1,2} \mathbf{a}_i(\vec{k}) \hat{e}_i(\hat{k}) e^{i(\vec{k} \cdot \vec{r} - \omega_0(\vec{k})t)}, \quad (5)$$

using the transverse base vectors

$$\hat{e}_1 = \hat{e}_z \times \hat{k} \quad \hat{e}_2 = \hat{e}_1 \times \hat{k}, \quad (6)$$

which is the decomposition that is usually used to quantize the photon field [11]. Any choice of basis vectors

$\hat{e}_1, \hat{e}_2$  in the plane transverse to  $\hat{k}$  is valid and does not play a role for the final result.

Calculating the electromagnetic fields from the ansatz yields the representations

$$\vec{E}(\vec{r}, t) = \int d^3k \vec{\mathbf{E}}_k e^{i(\vec{k} \cdot \vec{r} - \omega_0(\vec{k})t)} \quad (7)$$

$$\vec{B}(\vec{r}, t) = \int d^3k \vec{\mathbf{B}}_k e^{i(\vec{k} \cdot \vec{r} - \omega_0(\vec{k})t)} \quad (8)$$

with

$$\vec{\mathbf{E}}_k = \sum_{i=1,2} \mathbf{a}_i(\vec{k}) \hat{e}_i(\hat{k}) \omega_0(\vec{k}) \quad (9)$$

$$\vec{\mathbf{B}}_k = \sum_{i=1,2} \mathbf{a}_i(\vec{k}) \vec{\nabla} \times \hat{e}_i(\hat{k}). \quad (10)$$

### A. Fourier Transforms

When a Fourier transform of any of the Cartesian field components as they are output from a simulation is performed, we find, due to Hermiticity

$$F(-k) = F(k)^*, \quad (11)$$

where the  $*$  denotes complex conjugation. This means, that the two modes  $\vec{A}_k$ , propagating in  $\hat{k}$  direction, and  $\vec{A}_{-\vec{k}}$ , propagating in the opposite direction, are both contributing equally to  $F(\vec{k})$  and  $F(-\vec{k})$  and are thus indistinguishably mixed in the Fourier transform of any field component.

Mimicking this ambiguity, let us choose  $\vec{k}$  from any half space, e.g.  $k_x \geq 0$ , and superpose these two modes into a super-mode  $\vec{A}_k^s$

$$\vec{A}_k^s(\vec{r}, t) = \vec{A}_k(\vec{r}, t) + \vec{A}_{-\vec{k}}(\vec{r}, t). \quad (12)$$

From this, we can calculate the real electromagnetic fields that will result from this superposition

$$\vec{E}_k^s(\vec{r}, t) = -\Re \frac{\partial \vec{A}_k^s(\vec{r}, t)}{\partial t} \quad (13)$$

$$\vec{B}_k^s(\vec{r}, t) = \Re \vec{\nabla} \times \vec{A}_k^s(\vec{r}, t), \quad (14)$$

where  $\Re$  denotes taking the real part of a complex number.

In the world of simulation data we will find that the real Field modes are given by the superposition of the Hermitian conjugate modes

$$\vec{E}_k^F(\vec{r}) = \vec{\mathbf{E}}_k^F e^{i\vec{k} \cdot \vec{r}} + \vec{\mathbf{E}}_{-\vec{k}}^F e^{-i\vec{k} \cdot \vec{r}} \quad (15)$$

$$= 2\Re [\vec{\mathbf{E}}_k^F e^{i\vec{k} \cdot \vec{r}}] \quad (16)$$

$$\vec{E}_k^F(\vec{r}) = 2\Re [\vec{\mathbf{B}}_k^F e^{i\vec{k} \cdot \vec{r}}]. \quad (17)$$

If we now demand both representations to have equal field content we can require

$$\begin{aligned} \vec{B}_k^s(\vec{r}, 0) + \frac{1}{\omega_0(\vec{k})} \vec{k} \times \vec{E}_k^s(\vec{r}, 0) \\ = \vec{B}_k^E(\vec{r}) + \frac{1}{\omega_0(\vec{k})} \vec{k} \times \vec{E}_k^E(\vec{r}) \end{aligned} \quad (18)$$

and equate the coefficients of  $\sin(\vec{k} \cdot \vec{r})$  and  $\cos(\vec{k} \cdot \vec{r})$ . The resulting system of equations can be solved for  $\mathbf{a}_1(\vec{k})$ ,  $\mathbf{a}_2(\vec{k})$  and we find

$$\begin{aligned} \mathbf{a}_1(\vec{k}) = \frac{-i}{\omega_0(\vec{k})\sqrt{k^2 - k_z^2}} \times \dots \\ \left( \omega_0(\vec{k})\hat{e}_z \cdot \vec{\mathbf{B}}_k^F + (\vec{k} \times \vec{\mathbf{E}}_k^F)_z \right) \end{aligned} \quad (19)$$

$$\begin{aligned} \mathbf{a}_2(\vec{k}) = \frac{i}{\omega_0(\vec{k})k\sqrt{k^2 - k_z^2}} \times \dots \\ \left( k^2\hat{e}_z \cdot \vec{\mathbf{E}}_k^F - \omega_0(\vec{k})(\vec{k} \times \vec{\mathbf{B}}_k^F)_z \right), \end{aligned} \quad (20)$$

if we additionally assume  $\vec{k} \cdot \vec{\mathbf{E}}_k^F = 0$  and  $\vec{k} \cdot \vec{\mathbf{B}}_k^F = 0$  which are the Fourier domain equivalents of  $\vec{\nabla} \cdot \vec{E} = 0$  and  $\vec{\nabla} \cdot \vec{B} = 0$ . Please note that these are now the mode coefficients of the modes that propagate in  $\vec{k}$  direction without contributions of the opposite propagating mode, for any choice of  $\vec{k}$  from  $\mathbb{R}^3$ , as our choice of half-space in the beginning was arbitrary.

## B. The reconstructed $\vec{k}$ -space

To get to the final result we just need to plug the results Eqs. (19) and (20) into Eqs. (9) and (10) and find

$$\vec{\mathbf{E}}_k = \frac{1}{2} \vec{\mathbf{E}}_k^F - \frac{\omega_0(\vec{k})}{2k^2} (\vec{k} \times \vec{\mathbf{B}}_k^F) \quad (21)$$

$$\vec{\mathbf{B}}_k = \frac{1}{2} \vec{\mathbf{B}}_k^F + \frac{1}{2\omega_0(\vec{k})} (\vec{k} \times \vec{\mathbf{E}}_k^F). \quad (22)$$

These equations are similar to the projection operators defined in [12]. The difference is that, instead of projecting to two distinct subspaces with a specific propagation axis, we combine both parts to a combined, complex field which contains all the information at once.

At this point it is not yet clear which function we should plug in for  $\omega_0(\vec{k})$ . The possible choices are  $\omega_0(\vec{k}) = c|\vec{k}|$ , the dispersion relation of the vacuum, or  $\omega_0(\vec{k}) = \omega_{\text{grid}}(\vec{k})$ , the grid dispersion relation arising from whatever numerical solver we are using to create the data that we want to apply this method to. In Sec. III C we present the results of this method, applied to simulation data created by a traditional FDTD method [3] as implemented in the EPOCH [4] code, testing both options for  $\omega_0$ . The results clearly demonstrate that the

vacuum dispersion relation has to be used. Knowing this, we can further simplify Eqs. (21) and (22) and obtain

$$\vec{\mathbf{E}}_k = \frac{1}{2} \left( \vec{\mathbf{E}}_k^F - c\hat{k} \times \vec{\mathbf{B}}_k^F \right) \quad (23)$$

$$\vec{\mathbf{B}}_k = \frac{1}{2} \left( \vec{\mathbf{B}}_k^F + \frac{1}{c}\hat{k} \times \vec{\mathbf{E}}_k^F \right). \quad (24)$$

In the one dimensional case  $k_y = k_z = 0$  we find

$$\mathbf{E}_{y,k_x} = \frac{1}{2} (\mathbf{E}_{y,k_x}^F + \text{sgn}(k_x)c\mathbf{B}_{z,k_x}^F) \quad (25)$$

which is another formulation of the well known result Eq. (1) for electromagnetic plane waves in one dimension.

## C. Temporal evolution

The temporal phase terms in Eq. (4) are applicable directly to the reconstructed  $\vec{k}$ -space for any field component in order to evolve the field in time. Multiplying the complex amplitudes at each wave-vector  $\vec{k}$  with the temporal phase terms  $e^{-i\omega_0(\vec{k})\Delta t}$  will evolve fields by a time step  $\Delta t$  just as they would propagate in vacuum, according to Eqs. (7) and (8). This can be used to propagate the near field data into the far field, in order to be able to compare simulation results with experimental measurements or to calculate the boundary input necessary to obtain the desired laser focus in a simulation.

## III. NUMERICAL DETAILS

Applying the resulting Eqs. (21) and (22) to simulation data is straightforward, if the electric and magnetic fields are given on the same spatial grid and at the same physical time. Unfortunately, many codes use some kind of spatial staggering and/or temporal staggering.

### A. Spatial staggering

Spatial staggering means that different field components are defined on grids whose origins are shifted by half a grid spacing either in longitudinal or transverse direction. This needs to be reversed, such that the fields are defined on the same grid. If a discrete Fourier transform is performed anyway, it is straightforward to apply a linear phase term  $e^{i\vec{k}\vec{r}}$  to the various field components to remove the grid stagger. While this is the obvious solution, it might not always provide the highest precision.

### B. Temporal staggering

A lot of PIC codes use a leapfrog method. This means that various objects or properties thereof are updated in

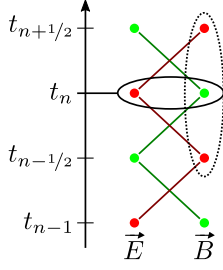


FIG. 1. The double leap-frog scheme of some PIC codes. Red dots represent the fields given by the original leap-frog scheme which is only concerned with the fields that are connected with the red lines. Green dots represent the additional fields that are calculated by the additional half-step updates. They form a second group of fields that are part of an implicitly emerging second leap-frog scheme, visualized by the green lines. Please note that, within the dashed ellipse, the field represented by the green dot  $B(t_n)$  is given by a linear interpolation between the fields represented by the red dots  $B(t_{n-1/2})$  and  $B(t_{n+1/2})$ . The fields within the solid ellipse are used to reconstruct the complex k-space at time  $t$ , because they are part of the same dump.

an alternating way. Especially for the electromagnetic fields this means that the electric and magnetic field are usually not calculated at the same physical time. While it might be possible to rework the deduction in the previous section to work with the fields at staggered times, this is not straightforward. On the other hand, it should be possible to obtain fields at consecutive step and interpolate to the required time by an adequate method. Some codes implicitly have routines in place, that will output the fields at equal times.

### C. The double leap-frog scheme

For example the EPOCH code [4] uses a split-step method that produces a double leapfrog scheme, see Fig. 1. The half-step fields output by EPOCH are basically the result of a linear interpolation, as can be shown from EPOCH's actual update equations [4].

A linear interpolation introduces a frequency response, since linear interpolation can be viewed as a discrete convolution (represented by the operator “\*”:  $(g * h)(n) = \sum_i x(i) * y(n+i)$ ) with the kernel  $[1-a, a]$  followed by a translation. For  $0 \leq a \leq 1$  we have

$$\begin{aligned} g(n) &= (1-a)f(n) + af(n+1) \\ &= ([1-a, a] * f)(n), \\ \tilde{f}(n+a) &= g(n) \\ &= (1-a)f(n) + af(n+1). \end{aligned}$$

This operation can be represented in frequency domain by multiplying with the discrete Fourier transform of the kernel

$$FT\{[1-a, a]\} = (1-a) + a e^{i\omega\Delta t}$$

and a linear phase  $e^{-i\omega a\Delta t}$  accounting for the translation, resulting in

$$FT\{\tilde{f}\} = e^{-i\omega a\Delta t} ((1-a) + a e^{i\omega\Delta t}) FT\{f\}. \quad (26)$$

In case of an interpolation by a half step,  $a = \frac{1}{2}$ , this simplifies to

$$FT\{\tilde{f}\}(\omega) = \underbrace{\cos\left(\frac{1}{2}\omega\Delta t\right)}_{=:R(\omega)} FT\{f\}(\omega). \quad (27)$$

Please note that this frequency response completely removes waves at the Nyquist frequency  $\omega_N = \frac{\pi}{\Delta t}$ . This frequency response  $R(\omega)$  is implicitly contained in any field that is produced by linear interpolating the Fields from neighbouring steps.

Performing a Fourier transformation of field data from a simulation dump from spatial domain to the frequency domain, the resulting spectrum is not a function of  $\omega$ , but a function of  $\vec{k}$ . In order to remove the frequency response, we have to use the grid dispersion relation  $\omega(\vec{k})$  in order to arrive at the spatial frequency response

$$\tilde{R}(\vec{k}) := R(\omega_{\text{grid}}(\vec{k})). \quad (28)$$

Since the time-step  $\Delta t$  of a PIC simulation is chosen such that all spatially resolved waves propagate with a frequency below the Nyquist frequency due to the CFL condition, the spatial frequency response  $\tilde{R}(\vec{k})$  is positive for any  $\vec{k}$  present in the discrete Fourier transform of the output fields. This means that we can divide the Fields by this function after performing the discrete Fourier transformation and, with respect to the spectrum, reverse the adverse effect of the linear interpolation. The only side effect is a slight amplification of noise.

The grid dispersion relation of simulations using Yee's scheme is given by

$$s_{\omega_{\text{grid}}}^2 = s_x^2 + s_y^2 + s_z^2$$

with the abbreviations

$$\begin{aligned} s_{\omega_{\text{grid}}} &= \frac{\sin\left(\frac{1}{2}\omega_{\text{grid}}\Delta t\right)}{c\Delta t}, \\ s_{\{x,y,z\}} &= \frac{\sin\left(\frac{1}{2}k_{\{x,y,z\}}\Delta\{x,y,z\}\right)}{\Delta\{x,y,z\}}. \end{aligned}$$

This can be used to find the explicit expression for the frequency response of the temporal linear interpolation, using the Yee solver dispersion relation

$$\tilde{R}(\vec{k}) = \sqrt{1 - c^2\Delta t^2 (s_x^2 + s_y^2 + s_z^2)}. \quad (29)$$

If the used solver scheme deviates from the standard Yee solver, a different dispersion relation needs to be plugged into Eq. (28). For other possible schemes see [13–16].

Correcting for the frequency response of the linear interpolation is now done by dividing the interpolated field (in the case displayed in Fig. 1, this is the  $\vec{B}$ -field), by  $\tilde{R}(\vec{k})$  in frequency domain, before using Eqs. (21) and (22).

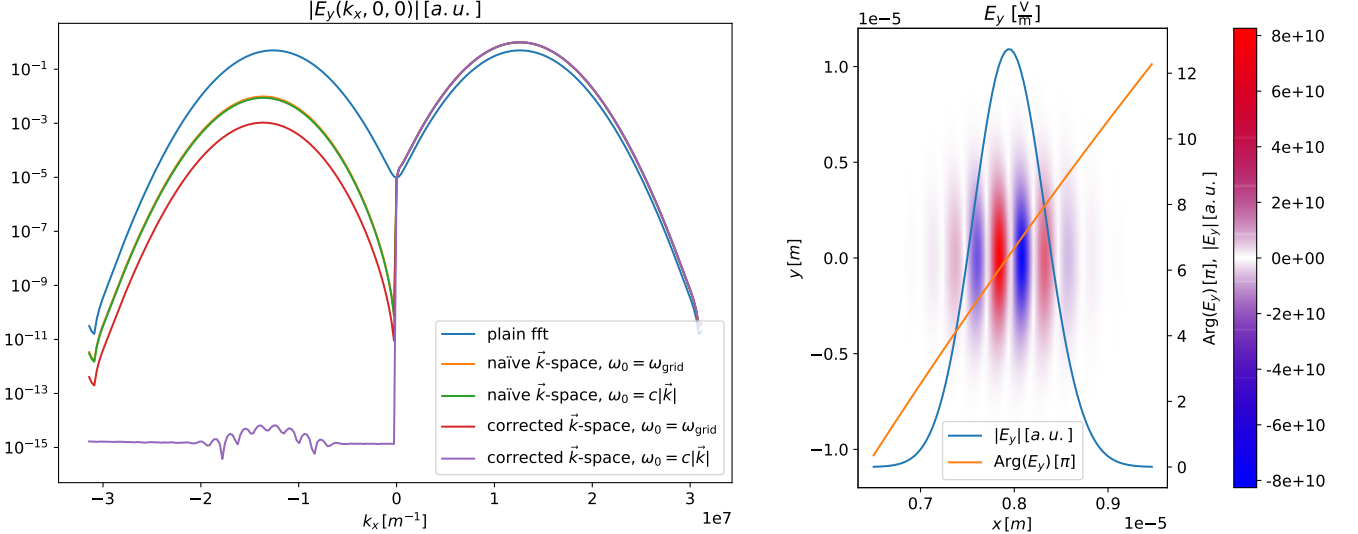


FIG. 2. Data from a simulation containing only a Gaussian pulse. Left figure: comparison between the spectra given by a simple fft, reconstructed  $\vec{k}$ -space with (“corrected”) or without correction (“naïve”) for the response function of the linear interpolation (by dividing the interpolated field by  $\tilde{R}(\vec{k})$  in frequency domain, see Eq. (29)), both combined with both options for  $\omega_0(\vec{k})$  in Eq. (21) each. The items in the figure legend are ordered according to the amplitude of the peak for negative  $k_x$ . The spectra are normalized to the maximum of the corrected  $\vec{k}$ -space. All but the plain Fourier transform overlap for positive  $k_x$ , indicating that all results basically agree on the right-moving part of the field, the small differences are invisible due to the logarithmic scaling. The difference between the methods is more visible for the negative  $k_x$  in that they have a different ability to demonstrate the absence of any left-moving part of the field. The two curves for the naïve method overlap, hiding the yellow curve almost completely. Both variants produce a left-moving ghost peak of about  $10^{-2}$  of the fields amplitude. The method that corrects for the linear interpolation response improves this to well below  $10^{-3}$  when using  $\omega_0(\vec{k}) = \omega_{\text{grid}}(\vec{k})$ . The corrected method using  $\omega_0(\vec{k}) = c|\vec{k}|$  is able to agree with the complete absence of any left-moving field up to 15 orders of magnitude (which is basically machine precision), shown as the purple curve. Right figure: envelope and phase (unwrapped using the algorithm described in [17]) of the pulse along the  $x$ -axis as retrieved by transforming the reconstructed  $\vec{k}$ -space back to spatial domain which yields the complex field.

#### IV. EXAMPLES

The methods described in the previous sections are implemented in PostPic [1, 2], an open source python package specifically designed to aid the evaluation of data from PIC simulations. This section will showcase the reconstruction of the physical  $\vec{k}$ -space from two distinct simulations performed with EPOCH. The first example will be a single Gaussian pulse in a 3D simulation without particles, the second example is a simulation of surface high harmonic generation (SHHG) at normal incidence.

##### A. Gaussian pulse

This example simulation was performed using EPOCH3D[4] on a  $720 \times 240 \times 240$  grid with a box size of  $24 \mu\text{m}$  in all directions. A laser source was placed at the  $x_{\min}$  boundary and set up with a wavelength of  $\lambda_l = \frac{1}{2} \mu\text{m} = 15\Delta x$ , a beam width of  $6.7 \mu\text{m}$  FWHM and pulse duration of  $3 \text{ fs}$  FWHM with its peak at  $8 \text{ fs}$  after beginning the simulation. From the grid dispersion relation we find that the laser propagates already

at  $\omega = 0.11 \omega_N$  and is subject to a frequency response  $\tilde{R}(k_l, 0, 0) = 0.98$ , reducing its amplitude in the interpolated field by about 2 percent.

In Fig. 2 the results for the reconstructed complex  $\vec{k}$ -space are shown. The simple fft, shown as a blue curve, does not distinguish between the peaks at  $k_l$  and  $-k_l$  and the spectrum is symmetric. Please note, that in Sec. II we left undefined, which function needs to be plugged in for  $\omega_0(\vec{k})$  in Eqs. (21)-(22) and two possible choices were proposed. Both options have been tested against this data. If the frequency response of the linear interpolation arising from EPOCHs half-step update is not taken into account, the contrast between the forward and backward propagating peaks is around 2 orders of magnitude. This can be understood, because the interpolation accounts for a mismatch of the electric and magnetic field amplitudes of 2 percent. The difference between the two options for  $\omega_0(\vec{k})$  is barely visible (orange and green curves) on the logarithmic scale. If the frequency response is corrected, the contrast between the peaks is greatly improved. Choosing  $\omega_0(\vec{k}) = \omega_{\text{grid}}(\vec{k})$  leads to one additional order of contrast (red curve), while in the case of

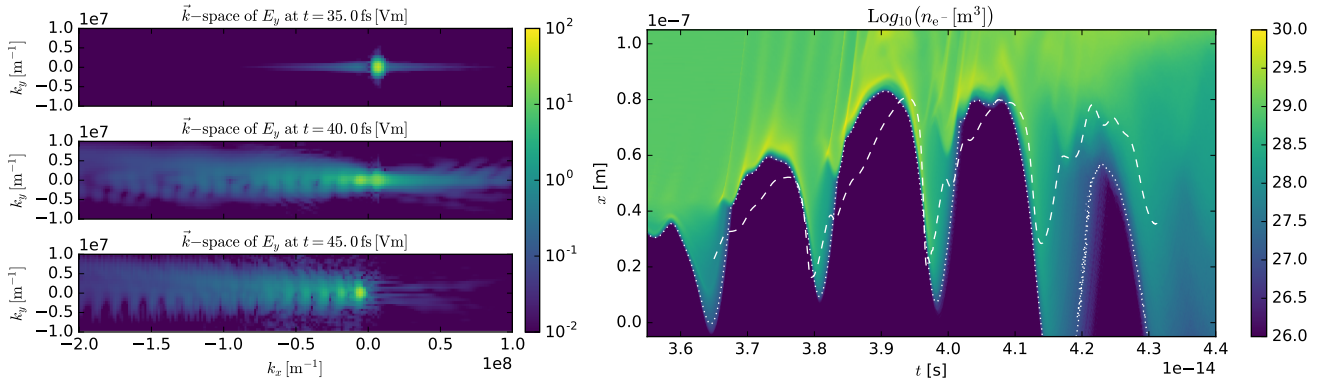


FIG. 3. Data from a simulation of surface high harmonic generation. Left figure: magnitude of the reconstructed  $\vec{k}$ -space in the beginning, middle and at the end of the interaction, from top to bottom. In the top figure it is clear that there is only the right-propagating laser pulse, with some residual side-lobes due to the finite extent of the used data. In the middle figure both are present, the leading edge of the left propagating harmonics and the tail of the incoming laser pulse. In the bottom figure only the left-propagating harmonics remain. Right figure: the apparent reflection point as reconstructed from the longitudinal phase of the outgoing waveform according to Eq. (30), calculated from the final dump only (dashed white curve). The background color scale indicates the plasma density. The motion of the apparent reflection point qualitatively resembles the motion of the plasma surface.

$\omega_0(\vec{k}) = c|\vec{k}|$  (purple curve), a contrast of 14 orders of magnitude is achieved. This indicates that this method has reached machine precision and that  $\omega_0(\vec{k}) = c|\vec{k}|$  clearly is the correct choice.

When the full  $\vec{k}$ -space is transformed back to the spatial domain via an inverse discrete Fourier transformation, the real part is basically identical to the original, real field from the output of the simulation. However, now the field also has an imaginary part that contains additional information, amplitude and phase. Now information about the spectral or temporal phase of a pulse is available readily from the data. The phase is of course wrapped to the interval  $[0, 2\pi]$  but unwrapping algorithms like the one described in [17] may be applied. Phase unwrapping has been applied to the phase data displayed on the right hand side of Fig. 2 yielding a perfectly linear phase.

## B. Surface High Harmonic Generation

When a high intensity laser pulse is reflected at a plasma surface, the plasma surface starts to move and distorts the reflected pulse. This distortion of the pulse shape accounts for the creation of high harmonics of the lasers fundamental frequency. The effect is called surface high harmonic generation, or SHHG for short. This simulation of surface high harmonic generation at  $0^\circ$  incidence was performed with EPOCH2d[4]. The size of the simulation box was set to  $12\ \mu\text{m}$  by  $10\ \mu\text{m}$  with 800 cells per  $\mu\text{m}$  in each direction. The laser was set to a wavelength  $\lambda_l = 1\ \mu\text{m}$  with a normalized intensity  $a_0 = 20$ . The spot size of the laser in focus on the target was set to  $2\ \mu\text{m}$  and the pulse duration to  $3\text{ fs}$  FWHM. The plasma density was set to  $n = 81n_c$  with an exponential ramp

with a scale length  $L = \frac{\lambda}{100}$ .

The reconstruction of the physical  $\vec{k}$ -space allows to separate the incident and outgoing waves at each time during the interaction, even when both are spatially superposed. In this two-dimensional case, the  $B_x$  field does not enter the  $\vec{k}$ -space reconstruction, due to  $k_z = 0$ , see Eq. (23). Thus, the results are based solely on the  $E_y$  and  $B_z$  fields. The resulting reconstructed  $\vec{k}$ -spaces are displayed on the left hand side of Fig. 3. From these results the left- and right-propagating waves can be separated by the sign of  $k_x$ . An animation of the fields during the interaction can be found online<sup>1</sup>.

Using the reconstruction of the physical  $k$ -space it is not only possible to separate incident and outgoing waves, it is also possible to gain access to the phase information of the waves. From the phase deviation of the outgoing field from the flat phase of the incident pulse, one may infer an apparent reflection point. Properly defining this apparent reflection point is not completely straightforward, but a simple approximate approach would be to start from the phase deviation  $\Delta\varphi$  and linearly scale it to an optical path length using the laser's spatial frequency  $k$ , resulting in

$$\Delta x = \frac{1}{2} \frac{\Delta\varphi}{k}. \quad (30)$$

Please note that Eq. (30) is a non-relativistic approximation and allows the apparent reflection point to move faster than the speed of light. The behaviour of the plasma surface and the apparent reflection point are displayed on the right hand side of Fig. 3. Both show qualitative agreement, but a full quantitative analysis would



<sup>1</sup> <https://youtu.be/JlygViEQL8g>

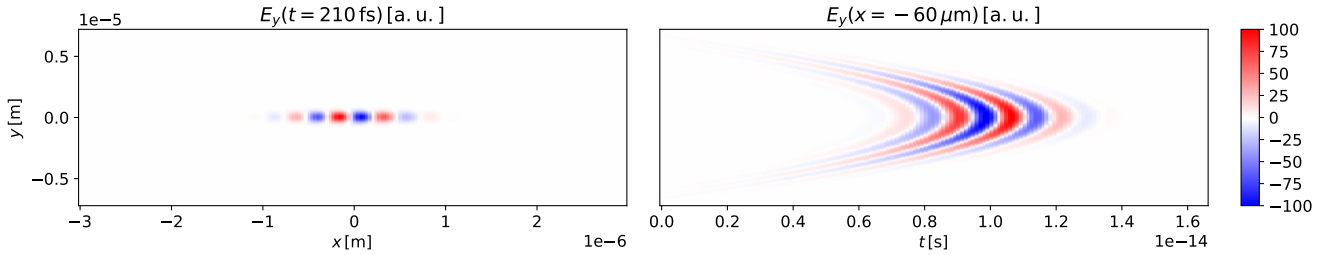


FIG. 4. Left figure: input field data of a narrow Gaussian focus at some point in time. These could be actual simulation or experimental data or created using a simple analytical model for the desired focus. Right figure: temporal profile at a boundary  $x = -60 \mu\text{m}$  that would reproduce the input field when used as input for a simulation, as computed by propagation via multiplication with a complex phase in the reconstructed  $\vec{k}$ -space. The desired pulse is first propagated backwards for 210 fs such that it lies left of the  $x = -60 \mu\text{m}$  boundary. After that, it is iteratively propagated forwards in steps of  $dt = \frac{dx}{c}$ , calculating the field at the boundary at each step.

require a better definition of the apparent reflection point that takes into account the relativistic motion of the plasma surface. This will be subject of a future publication. An animation of the plasma density and the apparent reflection surface during the interaction can be found online<sup>2</sup>.



### C. Temporal evolution in Fourier space

Using temporal evolution in Fourier space as briefly discussed in Sec. II C it is possible to calculate the boundary input necessary to achieve the desired focus field in a simulation. This is basically the same task as the calculation of the temporal field profile that will hit a detector that sits at a given plane. In order to do this, in initial (possibly negative)  $\Delta t$  is applied to the data such that the pulse lies just in front of the surface at which we would like to record the temporal profile. Please note that most of the calculations are performed in complex  $\vec{k}$ -space and it is not necessary to perform Fourier transforms at all steps. After that, the data is propagated iteratively in small steps  $dt = \frac{dx}{c}$  while recording the field at  $x = 0$  at each step. Due to the nature of the Fourier transform, in order to calculate the field at  $x = 0$  from the complex coefficients it is not necessary to calculate a full inverse Fourier transform, it is sufficient to sum up the data along the  $k_x$  axis, while leaving the  $k_y$  and  $k_z$  axis alone. This way we end up with a temporal profile in

the variables  $(t, k_y, k_z)$ . A 2D inverse Fourier transform of the  $(k_y, k_z)$ -plane may be optionally computed afterwards. An example of this is depicted in Fig. 4.

## V. CONCLUSION

The presented method is able to accurately reconstruct the physical  $\vec{k}$ -space from field data from simulations. Compared to earlier approaches, it requires only a single dump that contains the electromagnetic fields, which is easily available for most kinds of simulation. The method is computationally fast and a ready-to-use implementation is available as part of PostPic, an easy-to-use python package suitable for evaluation of many kinds of particle in cell simulation output files. This will hopefully lead to a more widespread use of  $\vec{k}$ -space analysis in various fields of physics that deal with simulations that contain electromagnetic fields, allowing easy access to spatial and temporal phases of all propagating waves in the simulation, even when counterpropagating waves are spatially superposed.

Connected to the main method described in this work is the possibility to do efficient temporal evolution of the fields dumped from a simulation. This provides access to far field data that can be compared with data collected by experiments, as well as supplying the necessary input data for simulations to recreate any kind of focal field configuration.

---

[1] S. Kuschel and A. Blinne, to be announced (2018).  
[2] PostPic Python Package, <https://www.github.com/skuschel/postpic> (2017).  
[3] K. S. Yee, IEEE Trans. Antennas Propag. **14**, 302 (1966).  
[4] T. D. Arber, K. Bennett, C. S. Brady, A. Lawrence-Douglas, M. G. Ramsay, N. J. Sircombe, P. Gillies, R. G. Evans, H. Schmitz, a. R. Bell, and C. P. Ridgers, Plasma Phys. Control. Fusion **57**, 113001 (2015).  
[5] S. V. Bulanov, N. M. Naumova, and F. Pegoraro, Phys. Plasmas **1**, 745 (1994).  
[6] R. Lichters, J. Meyer-ter Vehn, and A. Pukhov, Phys. Plasmas **3**, 3425 (1996).

<sup>2</sup> <https://youtu.be/U0RmoGLrgDk>

- [7] F. Quéré, C. Thaury, J.-P. Geindre, G. Bonnaud, P. Monot, and P. Martin, Phys. Rev. Lett. **100**, 095004 (2008).
- [8] U. Teubner and P. Gibbon, Rev. Mod. Phys. **81**, 445 (2009).
- [9] P. Heissler, R. Hörlein, M. Stafe, J. M. Mikhailova, Y. Nomura, D. Herrmann, R. Tautz, S. G. Rykovanov, I. B. Földes, K. Varjú, F. Tavella, A. Marcinkevicius, F. Krausz, L. Veisz, and G. D. Tsakiris, Appl. Phys. B **101**, 511 (2010).
- [10] P. Heissler, R. Hörlein, J. M. Mikhailova, L. Waldecker, P. Tzallas, A. Buck, K. Schmid, C. M. S. Sears, F. Krausz, L. Veisz, M. Zepf, and G. D. Tsakiris, Phys. Rev. Lett. **108**, 235003 (2012).
- [11] W. Greiner and J. Reinhardt, *Field Quantization* (Springer-Verlag, Berlin, Heidelberg, 1996).
- [12] M. Kolesik, J. V. Moloney, and M. Mlejnek, Phys. Rev. Lett. **89**, 283902 (2002).
- [13] A. Pukhov, J. Plasma Phys. **61**, 425 (1999).
- [14] B. M. Cowan, D. L. Bruhwiler, J. R. Cary, E. Cormier-Michel, and C. G. R. Geddes, Phys. Rev. Spec. Top. - Accel. Beams **16**, 041303 (2013).
- [15] R. Lehe, A. F. Lifschitz, C. Thaury, V. Malka, and X. Davoine, Phys. Rev. Spec. Top. - Accel. Beams **16**, 021301 (2013).
- [16] A. Blinne, D. Schinkel, S. Kuschel, N. Elkina, S. G. Rykovanov, and M. Zepf, Comput. Phys. Commun. (2017), 10.1016/j.cpc.2017.10.010.
- [17] M. A. Herráez, D. R. Burton, M. J. Lalor, and M. A. Gdeisat, Appl. Opt. **41**, 7437 (2002).